Original

Smetanin, M.; Deng, Q.; Weissmueller, J.:

Dynamic electro-chemo-mechanical analysis during cyclic voltammetry

In: Physical Chemistry Chemical Physics (2011) RSC Publishing

DOI: 10.1039/C1CP21781J

PCCP

Cite this: *Phys. Chem. Chem. Phys.*, 2011, **13**, 17313–17322

www.rsc.org/pccp

PAPER

Dynamic electro-chemo-mechanical analysis during cyclic voltammetry

Maxim Smetanin,*[a] Qibo Deng[a] and Jörg Weissmüller[ab]

Received 1st June 2011, Accepted 1st August 2011
DOI: 10.1039/c1cp21781j

We report and validate a method for measuring the strain-response, ς, of the electrode potential of electrically conductive solids in a fluid electrolyte. Simultaneously with cyclic voltammetry, the electrode is subjected to cyclic elastic strain at frequencies of up to 100 Hz. We explore three independent strategies for separating the cyclic variation of potential or current from the voltammogram proper, and find that the results of all three are in quantitative agreement. By means of an example we explore dominantly capacitive processes at a gold electrode in H_2SO_4 and $HClO_4$. The response parameter ς is not sensitive to the nature of the electrolyte. Yet, its value varies by more than a factor of two in the potential interval investigated. The potential of largest magnitude of ς agrees closely with the potential of zero charge.

Introduction

In this paper we report and validate a method for measuring the variation of the electrode potential, E, of electrically conductive solids, wetted by a fluid electrolyte, when the solid is elastically strained. More precisely, the parameter of interest is the electrode potential-strain coefficient, ς_E, defined *via* $\varsigma_E = \mathrm{d}E/\mathrm{d}e|_q$. Here q denotes the superficial charge density and e a tangential strain variable, to be defined below. At equilibrium, a Maxwell relation equates ς_E to another relevant thermodynamic parameter, the derivative of the surface stress, f, of the electrode with respect to its superficial charge density. In other words, $\varsigma_E = \varsigma_f$, where $\varsigma_f = \mathrm{d}f/\mathrm{d}q|_e$.[1] Furthermore, the electrode potential in the electrolyte is closely related to the electron work function of the surface in vacuum.[2,3] Therefore ς also agrees with yet another fundamental parameter, the work-function strain response. As we shall show, the response parameter varies significantly with E, and in the present paper we aim to establish a method for exploring the function $\varsigma(E)$ in the potential interval accessible to cyclic voltammetry.

The strain response of electrode potential or work function has long been of interest for problems as diverse as corrosion in structural materials under load[4,5] and the coupling of electronic properties to stress in semiconductor devices.[6–8] More recently, the suggestion[9] that a metal's catalytic activity should couple significantly to strain has prompted a renewed interest in the issue. Specifically, if E_a is the potential for a particular electrosorption process which is relevant for the catalytic reaction in question, then the variation of E_a with strain propagates into a strain response of the entire reaction.[10,11] Furthermore, the past decade has seen the advent of quantitative measurements of the surface stress of metal electrodes with a particular attention to the potential- or charge dependence of f. It has been suggested that the parameter ς_f provides information on the partial charge transfer between the metal and the adsorbate.[12]

Measurement of the potential variation with strain was first reported in early work by Gokhshtein (summarized by Valincius in ref. 13), who defined the response parameter, pointed out the Maxwell relation and proposed the 'estance' method as a technique for measuring $\varsigma_E(E)$. Yet, Gokhshtein's estance experiments did not see a detailed and comprehensive documentation in the literature, and key results remain either obscure—such as the numerical magnitude of ς_E and the procedure by which numbers were derived—or puzzling—such as the several sign changes of $\varsigma_E(E)$ in the potential range near zero charge. In fact, despite the fundamental relevance of the strain-response of the electrode potential, the phenomenon has remained poorly explored to this day. Reported numbers—including recent experiments—for the related quantity $\mathrm{d}E/\mathrm{d}\sigma$ (where σ is a measure for tangential stress in the bulk, which scales with e) differ by several orders of magnitude and even by sign.[1,5,14,21–23]

Until recently, the only confirmed quantitative experimental information on ς came from measurements of $\mathrm{d}f/\mathrm{d}q$. Experiments using cantilever bending or porous metal expansion measurements yield ς_f near the potential of zero charge (*pzc*) between −1 V and −2.5 V for various metal surfaces in weakly adsorbing electrolytes,[12,15–18] in agreement with *ab initio* work on ς_E.[19,20] Yet, a direct measurement of $\mathrm{d}E/\mathrm{d}e$ is desirable, especially in view of the nontrivial issue of equilibrium during real electrode processes. Recently, Smetanin *et al.*[21] reported an experiment which yields ς_E at the *pzc*, in quantitative agreement with *ab initio* simulation data[20] for the work-function strain response of Au in vacuum and with experimental data for ς_f of Au in the electrolyte.[12] In that work, a thin film

[a] *Institut für Werkstoffphysik und Technologie, Technische Universität Hamburg-Harburg, Hamburg, Germany. E-mail: maxim.smetanin@tu-harburg.de*
[b] *Institut für Werkstoffforschung, Werkstoffmechanik, Helmholtz Zentrum Geesthacht, Geesthacht, Germany*

electrode of Au on a flexible polymer substrate was cyclically strained under open circuit conditions. Smetanin *et al.* also discussed the important artefacts due to Faraday currents during slow strain cycles and the fundamental difference between experiments with polarisable electrodes, which are of interest in the present context, and those with nonpolarisable electrodes, which we ignore.[21–23]

The values of ς vary significantly, depending on the electrode process in question. For instance, the finding of $\varsigma \approx +1.5$ V for hydrogen underpotential deposition on Pd[10] contrasts with the negative-valued ς found for capacitive charging of transition metal surfaces. It is thus of interest to measure ς for different electrode processes, for instance during cyclic voltammetry.

Here we extend the approach of ref. 21, removing the restriction to open circuit conditions and including potential control. This allows us to measure $\varsigma_E(E)$ during cyclic voltammetry in large potential intervals. We describe the setup for this 'Dynamic Electro-Chemo-Mechanical Analysis' (DECMA) and report the results for gold electrodes in weakly adsorbing electrolytes, which can be verified by comparison to previously published data for $f(E)$ and for ς_E near the pzc.

Theory

Potential-strain response at equilibrium

In this section we briefly establish the terminology for discussing our experiments; for more details see the general discussion on electrochemical surface mechanics in ref. 1 and the detailed derivations in ref. 24.

We consider a polarisable electrode and introduce a surface free energy density, ψ, defined so that the net free energy of the electrode is

$$F = \Psi V + \psi A \tag{1}$$

with Ψ being the free energy density in the bulk. We measure the volume, V, and the surface area, A, for use with eqn (1) in coordinates of the reference configuration ('Lagrange coordinates'). Therefore, A does not change during the deformation, and ψ as well as the superficial charge density, q, are defined as densities per area of the surface in its undeformed state. A suitable strain variable, e, for use with isotropic surfaces is the relative change in the physical area, $\bar{A}$, during the deformation:

$$\delta e = \delta\bar{A}/\bar{A}. \tag{2}$$

The energy-conjugate variables to e and q defined in this way are the scalar surface stress, f, and the electrode potential, E. Thus,

$$\mathrm{d}\psi = f\,\mathrm{d}e + E\,\mathrm{d}q. \tag{3}$$

The state function ψ is related to the surface tension, γ, by a Legendre transform: $\gamma(e,E) = \psi(e,q) - qE$. The parameter of interest, the surface potential-strain coefficient ς_E, is a second derivative of ψ, namely

$$\varsigma_E = \mathrm{d}E/\mathrm{d}e|_q. \tag{4}$$

At equilibrium, the Maxwell relation equates ς_E to another important coefficient, the derivative of the surface stress with respect to the superficial charge density. In other words, $\varsigma_E = \varsigma_f$, where

$$\varsigma_f = \mathrm{d}f/\mathrm{d}q|_e. \tag{5}$$

Consider an experiment where e is varied cyclically with time, t:

$$e = e_0 \sin(\omega t) \tag{6}$$

with frequency ω and amplitude e_0. Consider further that the electrode is ideally polarisable (no Faraday processes) and that open circuit conditions apply. The potential will then vary as

$$E = E_0 \sin(\omega t) = \varsigma_E e_0 \sin(\omega t). \tag{7}$$

Therefore, ς_E can be obtained as the ratio of the amplitudes of E and e.

For use below, let us also consider an experiment where e is cycled at constant potential. Assuming small strain and a linear charge–strain relation, the charge density will vary according to

$$\delta q = \mathrm{d}q/\mathrm{d}e|_E\,\delta e \tag{8}$$

This variation may be related to ς_E by means of the identity[25] $\mathrm{d}X/\mathrm{d}Y|_Z = -\mathrm{d}X/\mathrm{d}Z|_Y\,\mathrm{d}Z/\mathrm{d}Y|_X$ for state variables X, Y, Z. In the present context, this implies

$$\mathrm{d}q/\mathrm{d}e|_E = -\mathrm{d}q/\mathrm{d}E|_e\,\mathrm{d}E/\mathrm{d}e|_q. \tag{9}$$

Since $\mathrm{d}q/\mathrm{d}E|_e$ represents the capacity, c, we have

$$\mathrm{d}q/\mathrm{d}e|_E = -\varsigma_E c. \tag{10}$$

Therefore, the charge density at equilibrium varies as

$$\delta q = -\varsigma_E c e_0 \sin(\omega t), \tag{11}$$

which implies that the net current density, j, varies as

$$j = \mathrm{d}q/\mathrm{d}t = j_0 \cos(\omega t) \tag{12}$$

with

$$j_0 = -\varsigma_E c e_0 \omega \tag{13}$$

or equivalently

$$I = \mathrm{d}Q/\mathrm{d}t = I_0 \cos(\omega t) \tag{14}$$

with

$$I_0 = -\varsigma_E C e_0 \omega \tag{15}$$

where I, Q, and C represent net current, net charge, and net capacity of the electrode, which are accessible in the experiment even when the electrode area is not known.

Potential strain response at finite frequency

In order to probe the potential-strain response in an experiment exploiting eqn (7), it is required that Faraday loss currents are sufficiently small so that q = constant is a good approximation. This can typically be enforced by performing the experiment at a sufficiently large strain frequency.[21,23] Such high-frequency strain cycles may lead to a limited equilibration, for instance due to the finite transport rate in

the electrolyte or due to slow adsorption rates. This leads to phase shifts in the potential- and/or current response that require separate discussion.

Let us again consider a cyclic strain $e_0 \sin(\omega t)$, as in eqn (6). When the current-strain response is linear, the potential variation at constant q and finite frequency will be

$$E = \varsigma^* e_0 \sin(\omega t - \phi) \quad (16)$$

with ς^* being an apparent response parameter and ϕ a phase shift. This cyclic potential variation gives rise to a cyclic current, which is again phase-shifted. As in conventional electrochemical impedance spectroscopy (EIS), potential and current are interrelated by the complex impedance, $\mathbf{Z} = Z_{re} - iZ_{im}$. The potential amplitude is here given by $\varsigma^* e_0$, and the potential signal is phase shifted by ϕ relative to the strain. The standard definition of the impedance[26] implies that the current signal is then

$$I = I_0 \cos(\omega t - \phi - \varphi) \quad (17)$$

with

$$I_0 = \varsigma^* e_0 / |\mathbf{Z}| \quad (18)$$

and

$$\tan \varphi = Z_{im}/Z_{re}. \quad (19)$$

It is important to note the analogy to conventional electrochemical impedance spectroscopy (EIS). The cyclic potential variation in a conventional EIS experiment is imposed by the potentiostat, and the impedance $\mathbf{Z}$ describes the response of the cyclic current. In dynamic electro-chemo-mechanical analysis, the potential variation is imposed by the cyclic strain, eqn (7), and the current-response is again governed by $\mathbf{Z}$. This implies that the function $\mathbf{Z}(\omega)$ can be measured by conventional impedance spectroscopy. Then, since $E_0 = \varsigma_E e_0$ (see eqn (7)), eqn (18) implies that

$$\varsigma^* = I_0 |\mathbf{Z}| / e_0. \quad (20)$$

In part of our work we exploited this relation, measuring I_0 in a DECMA experiment and combining the signal with the $\mathbf{Z}$ value as determined by an impedance spectroscopy experiment performed under nominally identical conditions in order to determine ς_E.

The experimental processes of interest are limited to surfaces with e near zero, and we therefore ignore the strain-dependence of the ς here. However, c and, as we shall show, ς vary significantly with E, and we aim to establish a method for exploring the function $\varsigma(E)$ in the potential interval accessible to cyclic voltammetry.

Experimental setup and procedures

Sample preparation

The working electrodes were 20 nm thin gold films thermally evaporated through a shadow mask unto 125 μm thick polyimide (Upilex®, UBE) substrates. Fig. 1b shows the sample geometry in top view. Prior to the metal deposition, the substrates were rinsed with ethanol and ultrapure water, dried in a nitrogen atmosphere, subjected to Ar plasma etching

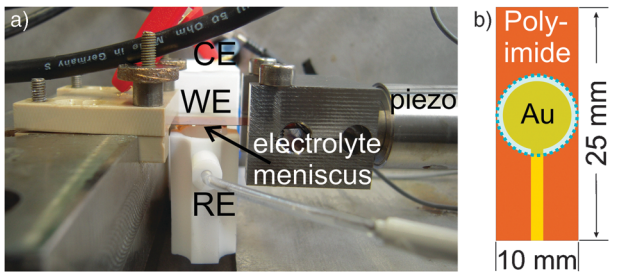

Fig. 1 Experimental setup. (a) The working electrode (WE) is attached to a fixed grip (left) and a mobile grip (right) which can be cyclically displaced by a piezoactuator. The electrochemical cell contacts the WE from below by a meniscus. Reference electrode (RE) is shown; counter electrode (RE) compartment is connected by a bridge and hidden from the view. The entire setup is housed in a high-vacuum grade stainless steel compartment under a protective atmosphere. (b) The WE is a patterned Au film on a polymer substrate. Shadowed blue disc with a dashed border line represents the contact area between the sample and the electrolyte.

for 5 min and then kept under 10^{-7} mbar vacuum for 12 h. Then 1–2 nm Ti was deposited as an adhesion promoter, followed by vapor deposition of the Au electrode proper at 0.02 nm s^{-1}. Before the electrochemical experiments, all samples used in this work were annealed for one hour in a vacuum of 10^{-8} mbar at 250 °C.

Dynamic electro-chemo-mechanical analysis stage

The mechanical setup (Fig. 1a) is identical to ref. 21 and is described in further detail in the thesis work of one of us.[27] The working electrode is clamped between a fixed and a mobile grip, the latter being cyclically displaced by a piezo actuator (Physical Instruments PI-840). The electrode is horizontal, with the metal facing down, and is wetted from below by a standing meniscus of electrolyte. Buckling of the electrode is prevented by a slight pretension. Typical displacement amplitudes are 10–20 μm, yielding strain amplitudes of order 10^{-4}. The entire mechanical and electrochemical setup is enclosed in an O-ring sealed, high vacuum type stainless steel casing that is repeatedly evacuated and flushed with high purity (99.999%) Ar and then sealed under Ar at atmospheric pressure during the experiment.

Electrochemical cells, made from Teflon or glass, consisted of the main body and a counter electrode (CE) compartment separated by a channel. Au wire was used as the CE.

The reference electrode, Ag/AgCl in 3.5 M KCl (World Precision Instruments), was separated from the main body of the cell by a Luggin capillary ending about 2 mm from the sample surface. All potentials in this work are quoted *versus* the standard hydrogen electrode (SHE), and are positive by 197 mV compared to potentials measured *versus* Ag/AgCl in 3.5 M KCl.[26]

The electrolytes were prepared from H_2SO_4, $HClO_4$ (Suprapur®, Merck) and ultrapure (18.1 MΩ cm, Sartotius) water and it was deaerated with 99.9999% Ar. Prior to the experiment, the electrochemical cell was placed into the cleaning solution (5 volume parts of concentrated H_2SO_4 + 1 part of 30% H_2O_2) for 24 h and then rinsed thoroughly with ultrapure water.

Measurement electronics

We used a potentiostat (PG-Stat 302N AUTOLAB) equipped with a grounded working electrode, a linear scan generator and an impedance module. Alternating current (AC) capacitance data were recorded *in situ* in the same cell and immediately preceding the cyclic strain experiments, but with the strain switched off. As an illustration of the results, an apparent capacitance, c^*, was evaluated from the imaginary part of the impedance as

$$c^* = 1/(i\omega Z_{\mathrm{Im}} A). \qquad (21)$$

The cyclic variation of potential or current in response to the strain cycles was measured by means of a lock-in amplifier (SR 7270 Signal Recovery) separately from the slower potential variation of the voltammogram, see below for details. The lock-in amplifier output for the in-phase ('real') and out-of-phase ('imaginary') amplitudes of a signal $S(t)$ is

$$s(t) = T^{1}\sqrt{2}\int_{t-T}^{t} \sin(\omega\tau - \phi)S(\tau)d\tau \qquad (22)$$

with $\phi = 0$ and $\pi/2$ for real and imaginary, respectively. T is the time constant. If the signal is a sine function, then the lock-in outputs need to be multiplied by $\sqrt{2}$ in order to obtain the amplitudes E_0 or I_0 described in the Theory section. The output of the displacement sensor (see below) was fed into the lock-in amplifier as the reference signal.

For synchronized data storage, the lock-in amplifier output signals were recorded as analog inputs by the potentiostat.

Measurement and control of strain

The piezo-actuator was operated in a closed-loop control mode. The grip displacement, δl, was recorded by a factory-calibrated displacement sensor integrated into the actuator system. The calibration factor, 6.00 ± 0.01 μm V^{-1}, was confirmed using a micrometer caliper.

The axial strain is $\delta l/l_0$ with l_0 being the initial sample length. Sufficiently far from the grips of a mechanical testing machine, the clamping constraints on the lateral deformation may be ignored and the stress approximated as uniaxial, of magnitude S_{U}. Hooke's law, along with the tendency of solids for transverse elastic contraction, implies that the total relative change in the surface area—which is the state variable in our theoretical framework—is $e = (1 - \nu)\delta l/l_0$. In the data analysis, we used $\nu = 0.35$ for the Poisson number of polyimide.[28]

It is essential that the metal film deforms elastically and coherently with the substrate. This condition was met, as was confirmed by the lack of hysteresis in $E(e)$ during slow cycles.[21] Note also that the strain amplitude never exceeded 10^{-3}, whereas *in situ* X-ray diffraction shows that similar films deform coherently with the substrate up to the much larger strain amplitude of 1%.[29]

Keeping the charge density constant

It is emphasized that the formalism of the Theory section relies on the use of Lagrange coordinates, see ref. 1. This means that the densities ψ and q are defined as the excess in free energy or charge, respectively, per area of the undeformed electrode surface. The experiment approximates open circuit conditions with a constant net charge. Let us assume that the wetted area in laboratory coordinates was kept constant during straining, for instance if the electrode–liquid–gas triple line would slip along the surface, thereby failing to follow the electrode movement. Then the net charge would be distributed over a variable area in referential coordinates, violating the condition of constant q and leading to an additional potential variation in the order of $\delta E \approx qc^{-1}\delta e$. Taking $q = c(E - E_{\mathrm{zc}})$, we estimate the additional contribution to the potential strain coefficient at $\delta E/\delta e \approx E - E_{\mathrm{zc}}$. This artifact is substantial and must be avoided.

In our experiment, constant charge density in referential coordinates was implemented by patterning the electrode so that it occupies only part of the wetted area of the polyimide film, see Fig. 1b. This geometry warrants that the entire electrode surface is wetted at all times. In this way, the charge resides on the same referential area (same atoms) irrespective of the strain.

The geometrical area of our electrodes was 0.62 ± 0.02 cm^2. Knowledge of the area is useful in the interest of comparing the magnitude of the capacitance to that of published data. It is emphasized, however, that the area is never a parameter in our experimental determination of ς.

Sample characterization

Scanning electron micrographs of the electrode surface (Fig. 2a) show an equilibrated grain structure with polygonal crystallites several hundred nm in size. This is confirmed by atomic force microscopy (AFM) images, shown in Fig. 2b, which display planar facets of 100–200 nm in size. The root-mean-square height variation is ~6 nm and the roughness factor, defined as the ratio between the real and projected surface area, is estimated at ~1.1. In view of the information from X-ray rocking curves (not shown, see ref. 12), which testify to a 111-orientation of the grains with an orientation spread of around 5°, the facets may be identified as 111-oriented.

Overview cyclic voltammograms in 10 mM $HClO_4$ (Fig. 3) are consistent with clean gold surfaces. Most CVs in this study are at an unusually small scan rate, so that even small Faraday currents show up prominently. It is emphasized that all results are compatible with clean electrolytes at low oxygen concentration, in spite of the noticeable Faraday current.

While the electrodes exhibit large (111)-facets, their defect density exceeds that of single crystals. Our choice was

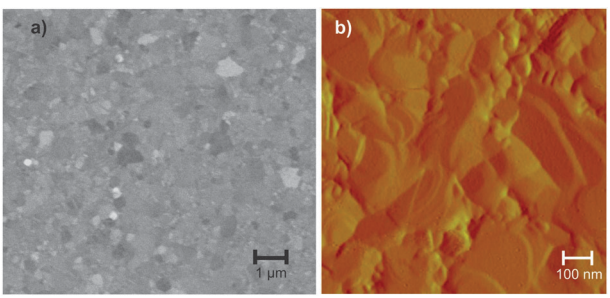

Fig. 2 Electrode surface topology. (a) Scanning electron micrograph. (b) Atomic force microscopy image of 1 × 1 μm area.

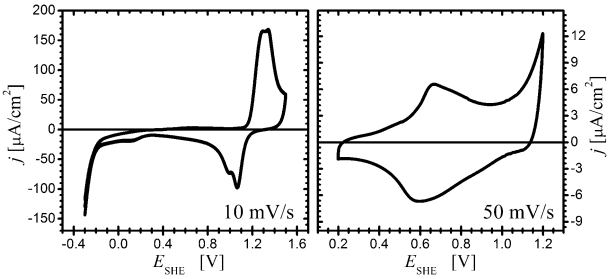

Fig. 3 Cyclic voltammograms of current density, j, *versus* electrode potential, E, in 10 mM $HClO_4$ and two different potential windows. Scan rates are indicated in the figures.

motivated by the need to apply a precisely quantifiable and purely elastic in-plane strain. Their strength and favorable geometry predestine thin films for this task. The use of single crystals would be less obvious, specifically due to their plastic yielding at low stress.

Measurement strategies and validation

Typical CVs in our study used linear potential scans with a scan rate of 1 mV s^{-1}, a potential interval of 1 V, and a total cycle time of around 30 minutes or 0.6 mHz. Strain cycles with frequencies, ω, of up to 100 Hz—up to 5 orders of magnitude faster than the potential cycle—were applied simultaneously. The amplitude of the strain-induced cyclic potential variation was in the order of 0.1–1 mV, much smaller than the potential range of the voltammogram. As detailed above, a lock-in amplifier was used to separate the two signals. Implementation of this scheme imposed two challenges: first, the potential variations on the two different time scales and with two quite different amplitudes need to be separated. Second, a distinguishing feature of cyclic voltammetry in potentiostatic mode is that the potentiostat controls the electrode potential at each time to the respective setpoint. Thereby, the potentiostat compensates and suppresses the very effect that is to be measured.

We have explored three different strategies to take account of these issues. We now show that quantitatively consistent results are obtained. Unless otherwise stated, the electrolyte was 10 mM $HClO_4$, and we used a potential scan rate of 1 mV s^{-1}, a strain frequency of 20 Hz with a strain amplitude of $e_0 = 2 \times 10^{-4}$.

Current-strain response in potentiostatic mode

In this setup, a conventional cyclic voltammogram is recorded while the electrode is cyclically strained. Even at $\omega = 100$ Hz, the strain cycles are sufficiently slow for the potentiostat to accurately compensate the strain-induced potential variation. This entails a cyclic modulation of the current, which can either be directly recorded as a part of the voltammogram or be analyzed in terms of amplitude and phase by the lock-in amplifier. We preferred the second alternative, since the first requires a high sampling rate for the current and leads to

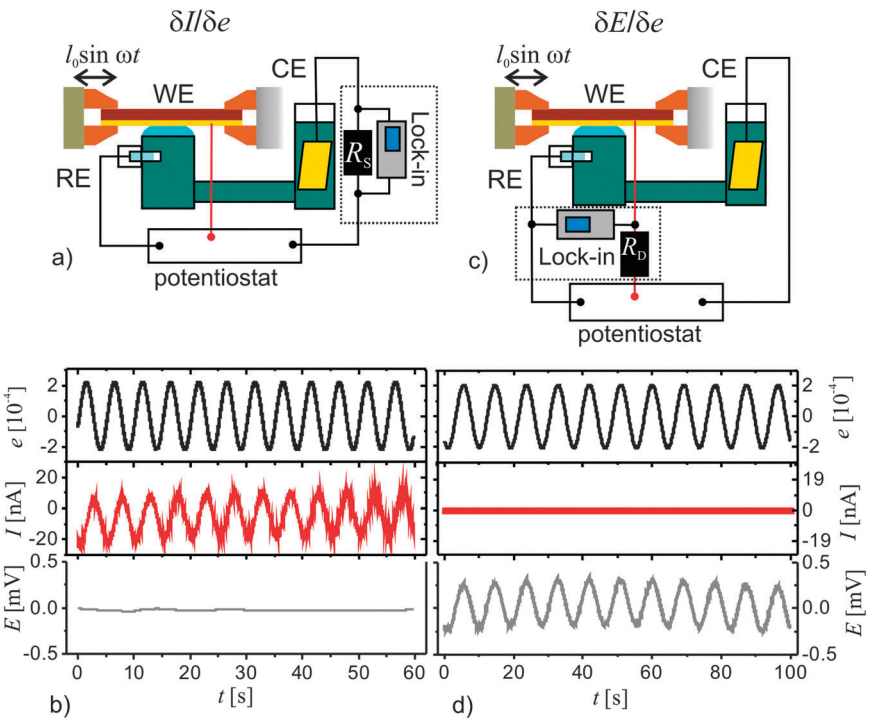

Fig. 4 Comparative display of experimental setups for current-strain response (left column) and potential-strain response (right column) during potentiostatic cyclic voltammetry in 10 mM $HClO_4$. Parts (a) and (c) in the top row are schematics of the electronics setup, showing counter, working, and reference electrodes (CE, WE, and RE), potentiostat as well as the shunt resistance R_S in (a) and the delay resistance R_D in (c). Parts (b) and (d) show oscilloscope traces of the relevant signals in the time (t) domain. Axis labeled E, I, and e refers to variations in electrode potential, electrode current, and elastic strain, respectively. Respective ordinate scales are identical in both columns. Note that potential variation is suppressed in the setup for current-strain response (a, c) while current variation is suppressed in the setup for potential-strain response (b, d).

prohibitively large data sets. According to eqn (20), the potential-strain coefficient can be determined from the current amplitude, provided that the impedance is also known. We have therefore performed AC-impedance measurements *in situ* and under identical conditions as the experiments with cyclic strain.

Fig. 4a illustrates the experimental configuration for this strategy. A shunt resistance of known magnitude, $R_S = 46\ \Omega$, was inserted between the potentiostat and the counter electrode, and the current amplitude I_0 was determined from the amplitude of the potential drop over R_S. By means of illustration we have imposed a constant potential and recorded the time-dependence of strain, current, and electrode potential by an oscilloscope. Fig. 4b shows the results. It is readily seen that E is held constant, in spite of the cyclic strain. It is also seen that the current variation is excellently resolved, in spite of the small strain amplitude.

Fig. 5 summarizes the results of the present strategy, starting out with the voltammogram (Fig. 5a) and the apparent capacitance values (Fig. 5b). Both graphs show a capacitance maximum at $E \approx 650$ mV *vs* SHE. Fig. 5c shows the amplitude, I_0, of the current modulation normalized to the strain amplitude, e_0. The graph appears similar to the capacitance curve, but a closer look reveals that the maximum of I_0/e_0 is at the potential 590 mV *vs*. SHE, 60 mV negative of the capacitance maximum. A similar deviation in the potentials of the respective maxima was found in all our experiments, see below.

By means of eqn (19) along with the experimental data for $|\mathbf{Z}|$ (Fig. 5b) one can determine ς_E from the current modulation and the impedance magnitude (as shown in Fig. 5b). Since the current modulation graph exhibits a slight hysteresis, the impedance data were measured during the positive- as well as negative-going potential scans and the respective branches used with eqn (20). The result (Fig. 5d) shows ς_E negative-valued in the entire potential range. For ease of comparison with the impedance and current modulation data, the negative of ς_E is plotted as the ordinate. Similar to c and I_0, the graph of $-\varsigma_E$ also exhibits a maximum. This feature is shifted to negative E relative to the peaks in $c(E)$ and, though to a much lesser amount, in $I_0(E)$.

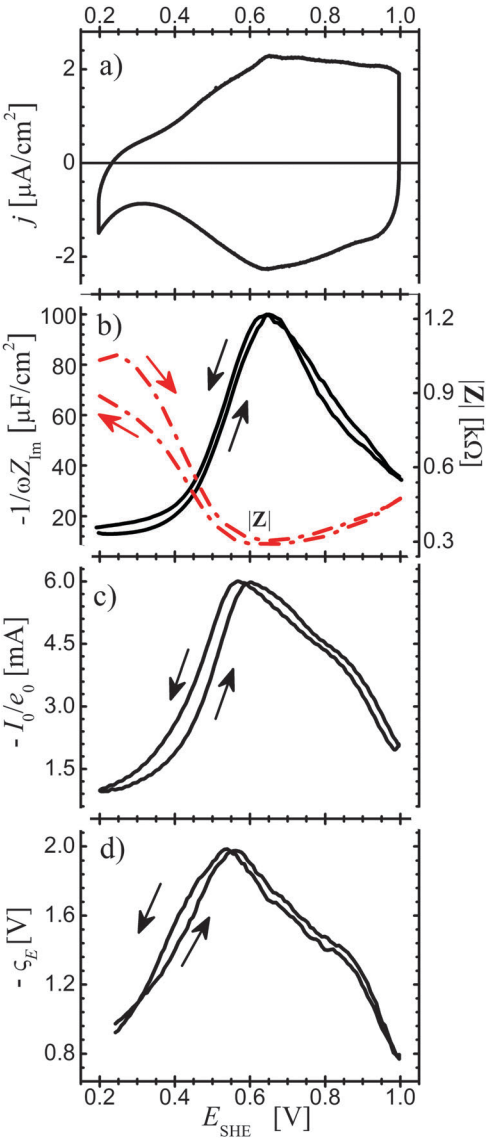

Fig. 5 Results of dynamic electromechanical analysis based on the current-strain response under potentiostatic control. (a) Cyclic voltammogram during the experiment recorded at 10 mV s^{-1}. (b) Apparent differential capacitance, $-1/(\omega Z_{Im})$. Also plotted (right ordinate) is the magnitude, $|\mathbf{Z}|$, of the impedance (red dashed line). (c) Current-strain response, I_0/e_0. (d) Potential–strain response computed *via* eqn (20). Electrolyte: 10 mM $HClO_4$, potential sweep rate: 10 mV s^{-1}, cyclic strain frequency: 20 Hz.

Potential-strain response in potentiostatic mode

Here, the experiment is modified so that ς_E can be measured directly, without the need of separate current response and capacitance data. To this end, a 'delay resistance', R_D, is connected in series with the working electrode (Fig. 4c). This resistance adds to the uncompensated solution resistance, R_U, which determines the potential drop between the RE and WE.[30] The result is an increase in the time constant for potential control at the WE, preventing the potentiostat from compensating the potential variation due to the cyclic straining. As a consequence, the strain-induced potential variation can be measured by a lock-in amplifier connected between the WE and CE.

By gradually increasing R_D we found that the current oscillation associated with the cyclic strain became negligible (*cf*. Fig. 4d) at $R_D \approx 50$ kΩ. For a typical electrode capacitance of $c = 100$ μF (compare Fig. 5b) this yields time constants of around 5 s, much longer than the cycle time of the mechanical strain but much shorter than the time to complete a sufficiently slow voltammogram. Electrochemical impedance spectroscopy suggested a solution resistance, R_U, of 350 Ω in our experiments. Even though $R_D \gg R_U$, cyclic voltammograms measured with and without the resistance R_D (Fig. 6a) exhibit only minor differences at the small scan rates in question.

Fig. 4d exemplifies the results for $e(t)$, $I(t)$, and $E(t)$ at an arbitrary chosen potential E and confirms the suppression of the cyclic current. This verifies that conditions of near constant

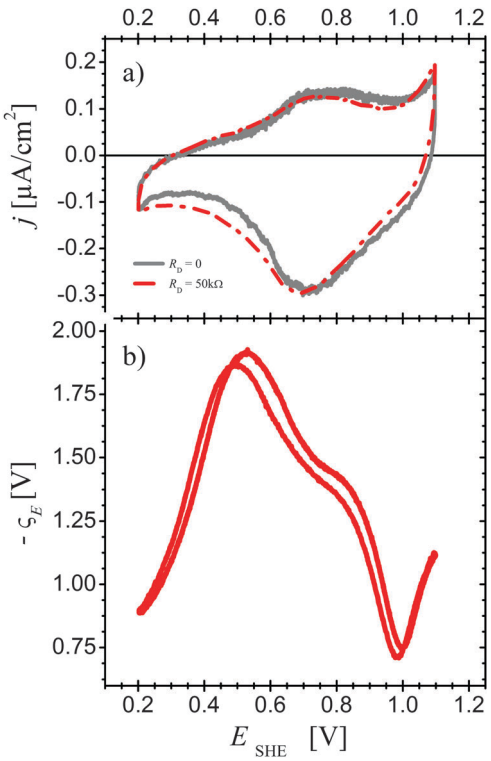

Fig. 6 Results of dynamic electro-chemo-mechanical analysis based on the potential-strain response under potentiostatic control in 10 mM $HClO_4$. (a) Cyclic voltammograms made without (—, gray solid curve) and with (– –, dashed red line) delay resistance R_D = 50 kΩ. Scan rate: 1 mV s^{-1}. (b) Potential-strain response measured during the cyclic voltammetry.

charge have been achieved, as required by the definition of ς_E. At the same time, the potential now acquires an oscillation caused by the cyclic strain of the electrode. A comparison of Fig. 4b and d illustrates the difference between the two measurement strategies of this and the previous subsection, notably the switch between constant potential and constant charge conditions.

Fig. 6b shows the result for ς_E obtained from the present strategy. The agreement with the results of Fig. 5d is apparent. The slightly larger hysteresis found here can be understood as the consequence of the delay resistance

Potential-strain response in galvanostatic mode

In galvanostatic mode, the current is controlled rather than the potential. For small current values and fast mechanical cycling, each cycle represents a process at constant charge. Here, the potential-strain response can be measured directly, without the need for a delay resistance. The drawback is the lack of control over the potential scan rate. We only briefly touch this method, which provides an additional verification of our procedures.

The lock-in amplifier was connected as in Fig. 4c, but the resistance R_D was removed. A galvanostatic cycle was executed between the current limits −1 μA and 1 μA with the current sweep rate of 10 nA s^{-1} and with cyclic strain applied. Fig. 7 shows the ς_E measured in this mode.

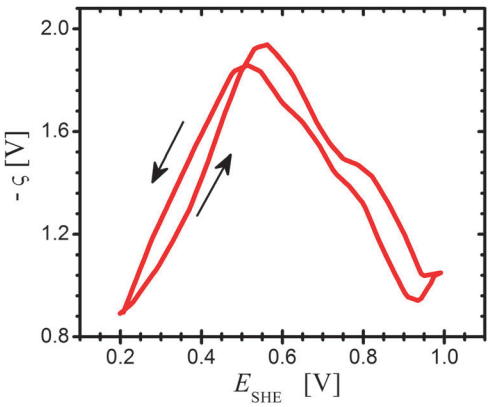

Fig. 7 Potential-strain response, ς_E, *versus* potential, E, measured in galvanostatic mode. Electrolyte is 10 mM $HClO_4$.

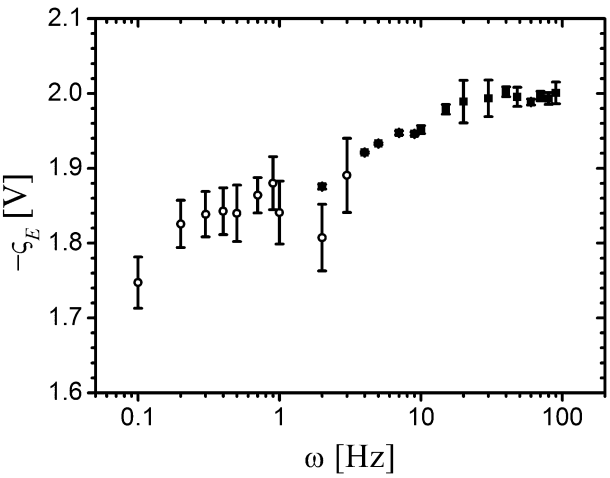

Fig. 8 Potential-strain response, ς_E, in 10 mM $HClO_4$ as the function of cyclic strain frequency, ω. Potential value is 547 mV, close to the maximum in $|\varsigma_E(E)|$. Measurement of ς_E uses chronopotentiometry under open circuit conditions (○) or potential-strain response using a lock-in amplifier (■).

Frequency dependence

Fig. 8 shows the dependence of ς_E in 10 mM $HClO_4$ on the cyclic strain frequency. In the higher frequency range (ω > 3 Hz) the measurement here used the potential-strain response method with the lock-in amplifier. The potential was E_1 = 547 mV, close to the potential of maximum $|\varsigma|$. At lower frequencies the data were recorded by means of chronopotentiometry under open circuit conditions after conditioning at E_1. During the measurement the potential here remained within few mV of E_1.

By inspection of Fig. 8 it is seen that the magnitude of ς_E increases slightly with ω, apparently saturating at and above 20 Hz.

Discussion

Fig. 9 summarizes the results for $\varsigma_E(E)$ from the three independent approaches. It is seen that the graphs agree, within narrow margins, throughout the entire potential range. We take this as a strong indication that our experiment provides valid data for the quantity of interest, the response

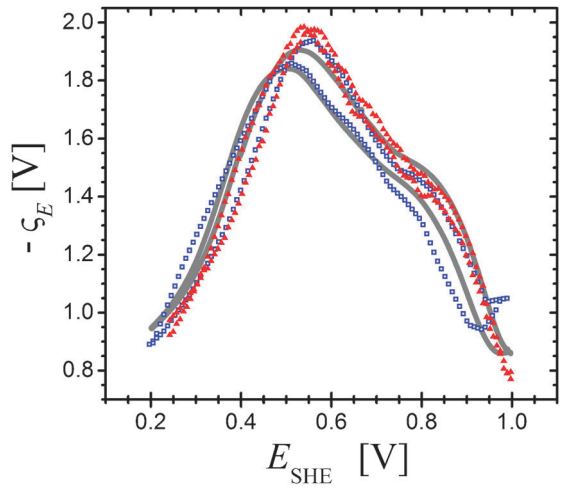

Fig. 9 Results of dynamic electro-chemo-mechanical analysis obtained using three methods: (▲) current strain response; (—) potential strain response and (▫) galvanostatic method. Note the excellent agreement.

of the electrode potential to strain at constant (Lagrangian) superficial charge density.

We now comment on the relative merits of the individual approaches.

Potential-strain response in galvanostatic mode

Here, charge and strain are controlled and the potential is measured. Therefore, this mode is most directly linked to the derivative in question, a potential variation with strain at constant charge. However, the drawback is the weak connection to the established voltammogram database, which is measured under conditions of controlled potential, not controlled current. Furthermore, the software of standard potentiostat systems does not lend itself to easy control of the vertex potential in galvanostatic mode.

Current-strain response in potentiostatic mode

Here, the current in response to strain is measured, and a separate measurement of the interfacial impedance is required to compute the potential-strain response by means of eqn (20). This strategy has the advantage of introducing a separate database (current modulation and capacity as opposed to potential variation), making the verification more meaningful. The drawbacks are twofold. First, there is a need for a separate impedance experiment. Second, and more importantly, the impedance measurement is not always conveniently done under identical conditions as the current modulation experiment. In our software (GPES 4.9 by Metrohm company), the potential is stepped and the impedance is measured at constant potential, typically for a succession of frequencies. By contrast, conventional cyclic voltammetry as well as our current modulation data involves—at least approximately—a continuously varying potential. Therefore, whenever there is hysteresis and/or scan-rate dependence in the electrode processes, the impedance data will not be measured at the same state of the electrode as the current modulation data. This difference is at odds with the requirements of eqn (20). The good agreement in the present instances shows that the above problem was only minor here, but this may not be generally true.

Potential-strain response in potentiostatic mode

This appears as the most practicable method, which will directly supply ς_E based on a single measurement. This measurement can be performed under identical conditions as a cyclic voltammogram. The obvious advantage is that features in ς_E can directly be related to the known features in the voltammogram. The need for a delay resistance appears as a drawback, since features in the voltammogram will be shifted on the potential axis. However, the impact on the voltammogram can be minimized when the mechanical cycling is fast and the potential scan rate is slow. In the present study, the delay resistance led to insignificant changes in the voltammogram.

Frequency dependence

The trend of $|\varsigma|$ increasing with increasing strain frequency agrees with earlier reports in ref. 21. There, the frequency dependence could be modeled as the consequence of Faraday loss currents, which violate the condition of constant q. The present data, however, vary much less with ω than what was found in the earlier work. The more stable behavior in the present experiments suggests a suppression of Faraday currents, which may be understood as the consequence of higher purity.

Application to different electrolytes

Results

Further dynamic electromechanical spectroscopy experiments studied identically prepared Au electrodes but different electrolytes. Fig. 10 summarizes results obtained with 1, 10 and 100 mM solutions of $HClO_4$ as well as H_2SO_4, again using strain cycles with the frequency of 20 Hz and the amplitude of $e_0 = 2 \times 10^{-4}$.

Our experiments show a sample-to-sample reproducibility in ς_E of $\sim$5%. To further enhance the comparability, all results for each of the two types of electrolytes were here obtained with the identical sample, in sequence of increasing concentration.

It is seen that the graphs of ς_E in $HClO_4$ and H_2SO_4 in Fig. 10 are quite similar. Their most prominent feature is the maximum in $|\varsigma_E|$. By averaging the potential, E_{max}, of the maximum over the electrolytes with different molarities and over both scan directions it is found that $E_{max} = 532 \pm 42$ mV in $HClO_4$ and $E_{max} = 532 \pm 40$ mV in H_2SO_4. Thus, the position of the maximum is independent of the electrolyte within narrow margins. E_{max} is invariably found negative of the potential of maximum capacitance as read from the CV's or from the impedance data (665 ± 20 mV in $HClO_4$ and 680 ± 20 mV in H_2SO_4). This confirms the observations described earlier in this paper.

It is also seen that all graphs exhibit shoulders at around 800 mV and an inversion in slope at around 1000 mV. These features are also quite reproducible and independent of the electrolyte.

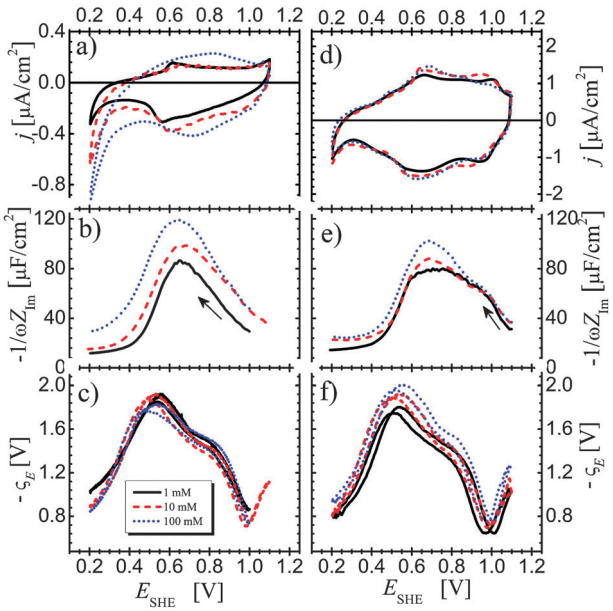

Fig. 10 Results of dynamic electro-chemo-mechanical analysis of the gold surface measured in $HClO_4$ (left column) and H_2SO_4 (right column). Top row: cyclic voltammograms recorded *in situ*. Center row: apparent differential capacitance. Bottom row: response parameter, ς, measured *via* potential-strain response under potentiostatic control. Potential sweep rate: 1 mV s^{-1} in $HClO_4$ and 5 mV s^{-1} in H_2SO_4; frequency for impedance and potential-strain measurements, 20 Hz. Concentration of $HClO_4$ and H_2SO_4 depicted as: 1 mM—solid black line, 10 mM—dashed red line, 100 mM—dashed blue dots.

The most notable difference between the results of perchloric and sulfuric acid is the concentration-dependence: as the function of molarity, the scans in $HClO_4$ exhibit a noticeable variation in capacitance but practically no variation in ς_E. By contrast, scans in H_2SO_4 give lesser capacitance variation yet a noticeable variation in ς_E.

Discussion

Our experiments indicate that the graphs of $\varsigma_E(E)$ in $HClO_4$ and H_2SO_4 are in close agreement. These graphs are also at most weakly dependent on the electrolyte concentration. The value of $\varsigma_E(E)$ at the extremum, -1.9 ± 0.2 V in $HClO_4$, agrees with our previously reported findings for ς_E at the open circuit potential (*ocp*).[21]

The graphs of $\varsigma(E)$ of gold in the present work show identical sign in a wide potential interval around the *pzc*. This is remarkable in view of the several sign changes reported by Gokhshtein for Pd and Pt electrodes. Studies of those metals with our technique are in preparation. In the meantime we note that measurement of surface stress *versus* charge for Au,[12,17] Pt[31,32] and Pd[33] testifies to a monotonously decreasing $f(q)$ within the range of dominantly capacitive charging. Since $\varsigma_E = \varsigma_f$ (*cf.* the Introduction), the observations for $f(q)$ are consistent with the present findings.

Several authors have reported a dependency of the value of ς near the *pzc* on an effective strength of adsorption. When this latter parameter was varied, either by varying the ion[16] or the concentration,[34] stronger adsorption was found to entail a smaller magnitude of ς. The observation has been linked to charge transfer between the electrode and the adsorbate and to the electrosorption valency.[12,16] The present observations do not confirm that picture. The finding, that ς is essentially independent of the ion and of the solution concentration, appears to link ς exclusively to the behavior of the metal surface.

The data also offer no apparent link between the potential-dependence of ς and simple concepts of the double-layer behavior near the *pzc*. For instance, the potential of maximum $|\varsigma|$ is near the potential of maximum capacitance, but the offset between the two potentials appears significant, preventing explanations based on a one-to-one correlation between ς and c.

The most obvious empirical correlation to the known electrode processes is the good agreement between the potential of maximum ς and the potential of zero charge. Within error bars, our value of E_{max} agrees with the *pzc* of Au(111) in $HClO_4$, 560 mV,[35] and in solutions containing SO_4^{2-}, $\sim$500 mV.[36] Note that the electrocapillary maximum of the surface tension is a forceful result of thermodynamics. By contrast, thermodynamics will neither require nor rule out an extremum of $\varsigma(E)$ near the *pzc*. Such behavior might then be specific to gold surfaces. Yet, if the finding was confirmed, and if the controlling role of the metal in the surface potential-strain response was taken at face value, then the extremum of $\varsigma(E)$ would provide a useful probe of the pzc of gold, which could be applied in general in electrochemical studies.

Irrespective of the above issue, an interpretation of $\varsigma(E)$ as a signature of the metal surface imposes the question of the origin of the dependency on potential or superficial charge density. One might speculate about band-filling by the excess charge, and in fact the issue would seem to be open to investigation by *ab initio* density functional theory approaches such as those of ref. 19, 20, 37 and 38.

Summary

We have explored three different strategies to investigate the electromechanical response during cyclic voltammetry. When applied to gold electrodes in weakly adsorbing electrolytes, all three strategies provide consistent results for the response, $\varsigma_E(E)$, of the electrode potential to elastic strain at constant superficial charge density. The findings also agree with earlier experimental and computational studies, which were restricted to ς_E at the potential of zero charge or at the open-circuit potential. The agreement of the various methods validates our analysis of the underlying science and shows that dynamic electro-chemo-mechanical analysis may be used as a tool for characterizing electrode processes.

As a case-study we have applied the new method to gold electrodes in $HClO_4$ and H_2SO_4 of different concentrations. The most obvious observation is a peak in the magnitude of ς_E at a potential which coincides with the *pzc*. Furthermore, the experimental graphs of $\varsigma_E(E)$ are at best weakly dependent on the nature of the electrolyte, suggesting that the experiment probes the signature of electronic processes in the metal surface. This would predestinate the method as a tool for separating processes within the electrode from those related to

electrosorption or to the behavior of the diffuse layer. Such processes are not readily separated by the more standard techniques such as cyclic voltammetry.

Acknowledgements

This work was supported by Deutsche Forschungsgemeinschaft under grant WE 1424/13. Q.D. acknowledges support by the China Scholarship Council.

References

1 D. Kramer and J. Weissmüller, *Surf. Sci.*, 2007, **601**, 3042.
2 S. Trasatti, *J. Electroanal. Chem.*, 1971, **33**, 351.
3 D. L. Rath and D. M. Kolb, *Surf. Sci.*, 1981, **109**, 641.
4 R. E. Fryxell and N. H. Nachtrieb, *J. Electrochem. Soc.*, 1952, **99**, 495.
5 Á. Horváth and R. Schiller, *Phys. Chem. Chem. Phys.*, 2001, **3**, 2662.
6 M. Ieong, B. Doris, J. Kedzierski, K. Rim and M. Yang, *Science*, 2004, **306**, 2057.
7 R. Zallen and W. Paul, *Phys. Rev.*, 1967, **155**, 703.
8 Y. S. Choi, T. Numata, T. Nishida, R. Harris and S. E. Thompson, *J. Appl. Phys.*, 2008, **103**, 064510.
9 M. Mavrikakis, B. Hammer and J. K. Nørskov, *Phys. Rev. Lett.*, 1998, **81**, 2819.
10 L. A. Kibler, E. M. El-Aziz, R. Hoyer and D. M. Kolb, *Angew. Chem., Int. Ed.*, 2005, **44**, 2080.
11 J. Weissmüler, R. N. Viswanath, L. Kibler and D. M. Kolb, *Phys. Chem. Chem. Phys.*, 2011, **13**, 2114.
12 M. Smetanin, R. N. Viswanath, D. Kramer, D. Beckmann, T. Koch, L. A. Kibler, D. M. Kolb and J. Weissmüller, *Langmuir*, 2008, **24**, 8561.
13 G. Valincius, *J. Electroanal. Chem.*, 1999, **478**, 40.
14 P. P. Craig, *Phys. Rev. Lett.*, 1969, **22**, 700.
15 H. Ibach, C. E. Bach, M. Giesen and A. Grossmann, *Surf. Sci.*, 1997, **375**, 107.
16 W. Haiss, R. J. Nichols, J. K. Sass and K. P. Charle, *J. Electroanal. Chem.*, 1998, **452**, 199.
17 N. Vasiljevic, T. Trimble, N. Dimitrov and K. Sieradzki, *Langmuir*, 2004, **20**, 6639.
18 J. Weissmüller, R. N. Viswanath, D. Kramer, P. Zimmer, R. Würschum and H. Gleiter, *Science*, 2003, **300**, 312.
19 F. Weigend, F. Evers and J. Weissmüller, *Small*, 2006, **2**, 1497.
20 Y. Umeno, C. Elsässer, B. Meyer, P. Gumbsch, M. Nothacker, J. Weissmüller and F. Evers, *Europhys. Lett.*, 2007, **78**, 13001.
21 M. Smetanin, D. Kramer, S. Mohanan, U. Herr and J. Weissmüller, *Phys. Chem. Chem. Phys.*, 2009, **11**, 9008.
22 A. Horváth, G. Nagy and and R. Schiller, *Phys. Chem. Chem. Phys.*, 2010, **12**, 7290.
23 M. Smetanin, Q. Deng, D. Kramer, S. Mohanan, U. Herr and J. Weissmüller, *Phys. Chem. Chem. Phys.*, 2010, **12**, 7291.
24 J. Weissmüller and D. Kramer, *Langmuir*, 2005, **21**, 4592.
25 H. B. Callen, *Thermodynamics and an Introduction to Thermostatistics*, Wiley, New York, 2nd edn, 1985.
26 A. J. Bard and L. R. Faulkner, *Electrochemical Methods*, Wiley, New York, 2nd edn, 2001.
27 M. Smetanin, *Mechanics of the Electrified Interfaces in Diluted Electrolytes*, *PhD Thesis*, Universtät des Saarlandes, 2010. http://scidok.sulb.uni-saarland.de/volltexte/2010/3380/.
28 J. Dolbow and M. Gosz, *Mech. Mater.*, 1996, **23**, 314.
29 B. Özkaya, S. R. Saranu, S. Mohanan and U. Herr, *Phys. Status Solidi A*, 2008, **205**, 1876.
30 J. R. Macdonald, *Impedance Spectroscopy*, Wiley, 1987, §11.2.
31 R. N. Viswanath, D. Kramer and J. Weissmüller, *Electrochim. Acta*, 2008, **53**, 2757.
32 H. J. Jin, X. L. Wang, S. Parida, K. Wang, M. Seo and J. Weissmüller, *Nano Lett.*, 2010, **10**, 187.
33 G. R. Stafford and U. Bertocci, *J. Phys. Chem. C*, 2009, **113**, 13249.
34 R. N. Viswanath, D. Kramer and J. Weissmüller, *Langmuir*, 2005, **21**, 4604.
35 D. M. Kolb and J. Schneider, *Electrochim. Acta*, 1986, **31**, 929.
36 Z. Shi, J. Lipkowski, M. Gamboa, P. Zelenay and A. Wieckowski, *J. Electroanal. Chem.*, 1994, **366**, 317.
37 A. Y. Lozovoi and A. Alavi, *Phys. Rev. B: Condens. Matter*, 2003, **68**, 245416.
38 Y. Umeno, C. Elsässer, B. Meyer, P. Gumbsch and J. Weissmüller, *Europhys. Lett.*, 2008, **84**, 13002.

